Andrade and Critical Time-to-Failure Laws in Fiber-Matrix Composites: Experiments and Model

H. Nechad[1], A. Helmstetter[2], R. El Guerjouma[1] and D. Sornette[2,3,4]

[1] GEMPPM Groupe d'Etude de Métallurgie Physique et de Physique des Matériaux,
CNRS UMR5510 and INSA de Lyon, 20 Avenue Albert Einstein, 69621 Villeurbanne Cedex, France

[2] Institute of Geophysics and Planetary Physics,
University of California, Los Angeles, California 90095

[3] Department of Earth and Space Science,
University of California, Los Angeles, California 90095

[4] Laboratoire de Physique de la Matière Condensée
CNRS UMR6622 and Université de Nice-Sophia Antipolis,
B.P. 71, Parc Valrose, 06108 Nice Cedex 2, France

February 2, 2008

Abstract

We present creep experiments on fiber composite materials. Recorded strain rates and acoustic emission (AE) rates exhibit both a power law relaxation in the primary creep regime and a power-law acceleration before global failure. In particular, we observe time-to-failure power laws in the tertiary regime for acoustic emissions over four decades in time. We also discover correlations between some characteristics of the primary creep (exponent of the power-law and duration) and the time to failure of the samples. This result indicates that the tertiary regime is dependent on the relaxation and damage processes that occur in the primary regime and suggests a method of prediction of the time to failure based on the early time recording of the strain rate or AE rate. We consider a simple model of representative elements, interacting via democratic load sharing, with a large heterogeneity of strengths. Each element consists of a non-linear dashpot in parallel with a spring. This model recovers the experimental observations of the strain rate as a function of time.

Keywords: creep, rupture, Andrade law, acoustic emission, composites, time-to-failure singularity, fiber bundle models, shear-thinning rheology, Eyring rheology

1 Introduction

Time-dependent deformation of a material subjected to a constant stress level is known as creep. In creep, the stress is below the mechanical strength of the material, so that the rupture does not occur upon application of the load. It is by waiting a sufficiently long time that the cumulative strain may finally end in catastrophic rupture. Creep is all the more important, the larger the applied stress and the higher the temperature. The time to creep rupture is controlled by the stress sign and magnitude, temperature and microstructure. Since past decades, people have studied the creep rupture phenomena through direct experiments (Liu and Ross, 1996; Guarino et al., 2002; Lockner, 1998) as well as through different models (Miguel et al., 2002, Ciliberto et al., 2001; Kun et al., 2003; Hidalgo et al., 2002; Main, 2000; Politi et al., 2002; Pradhan and Chakrabarti, 2004; Turcotte et al., 2003; Shcherbakov and Turcotte, 2003; Vujosevic

and Krajcinovic, 1997; Saichev and Sornette, 2003). If a lot of works were devoted to homogeneous materials like metals (Ishikawa et al., 2002) and ceramics (Goretta et al., 2001; Morita and Hiraga, 2002) many recent studies concerns heterogeneous materials like composites and rocks (Liu and Ross, 1996; Guarino et al., 2002; Lockner, 1998). The knowledge of the failure properties of composite materials are of great importance because of the increasing number of applications for composites in engineering structures. The long-term behavior of these materials, especially polymer matrix composites is a critical issue for many modern engineering applications such as aerospace, biomedical and civil engineering infrastructure. Viscoelastic creep and creep-rupture behaviors are among the critical properties needed to assess long-term performance of polymer based composite materials. The knowledge of these properties is also required to design material microstructures which can be used to construct highly reliable components. For heterogeneous materials, the underlying microscopic failure mechanism of creep rupture is very complex depending on several characteristics of the specific types of materials. Beyond the development of analytical and numerical models, which predict the damage history in terms of the specific parameters of the constituents, another approach is to study the similarity of creep rupture with phase transitions phenomena (Andersen et al., 1997).

Creep is often divided into three regimes: (i) the primary creep regime corresponds to a decay of the strain rate following the application of the constant stress according to the so-called Andrade's law corresponding to a power law decay with time (Andrade, 1910); (ii) the secondary regime describes a quasi-constant strain rate, which evolves towards the (iii) tertiary creep regime in which the strain rate accelerates up to rupture. Andrade's law is similar to the power-law relaxation of the seismic activity ("aftershocks") triggered by the static stress change induced by a large earthquake, known as Omori's law (Omori, 1894). A power-law acceleration of seismicity has been reported before several large individual earthquakes (Sykes and Jaumé, 1999; Sammis and Sornette, 2002) but is not systematically observed. In contrast with rupture experiments, the acceleration of seismic activity before an earthquake is observed systematically only when averaging over many sequences. This average acceleration can be explained by the physics of earthquake triggering (Helmstetter et al., 2003). Rupture experiments performed at constant stress rate or strain rate can also produce a power-law acceleration of acoustic emission before failure (Anifrani et al., 1995; Garcimartin et al., 1997; Guarino et al., 2002; Johansen and Sornette, 2000). This power-law singularity may have a different origin than creep failure. For instance, critical rupture at constant stress rate occurs in networks of purely elastic elements with a heterogeneous distribution of strengths (Daniels, 1945).

The purpose of the present work is to present new experiments on well-controlled fiber composite materials and to explain these experiments, using a simple model of representative elements in the framework of fiber bundles models (Daniels, 1945). In our model, each element of the system interacts via democratic load sharing, and is characterized by a rupture threshold with a large heterogeneity of strengths. Our emphasis is in obtaining a complete description of all three regimes at the same time, viewed simultaneously from strain measurements as well as non-destructive acoustic emission recordings. Our approach strives to determine the crucial physical ingredients to capture the complete phenomenology observed in the experiments. The organization of the paper is the following. Section 2 presents the experimental design. Section 3 describes the experimental results for the strain rate and acoustic emission data. Section 4 presents our modeling effort, with a series of three models, from the simplest to the most relevant for our experiments. Section 5 concludes.

2 Experimental design

2.1 Materials and preparation of the samples

The experimental work is carried out on two types of angle cross ply glass/polyester composite materials, and on Sheet Molding Compound (SMC) composites. For all the composites, E glass fibers are used. The density of the fibers is 2.6 g/cm^3. Its tensile strength and modulus are 3.2 and 76 GPa, respectively. Rectangular plates of angle cross ply composites are obtained by a hand lay up technique in the lab. This method consists in applying successively into a mold surface a release agent, a layer of resin, a layer of unidirectional reinforcement and to impregnate the reinforcement by hand by means of a roller. Two cross angle ply laminates denoted $[\pm 62^o]_{12}$ and $[90^o/35^o]_{12}$ are thus fabricated. The angles are measured with respect to the loading direction as shown in Figure 1. The stacking sequence consists of 12 layers. Polymerization is achieved at room temperature during approximately 12 hours under pressure. The fiber volume fraction is 75%.

The SMC composites are of commercial quality. They consist of a combination of polyester resin, calcium carbonate filler, thermoplastic additive and random oriented short glass fibers, in the form of a sheet. The sheet contains all the components needed for molding the final part (resin, reinforcement, filler, catalyst, low profile additives, etc.) in a malleable and non-tacky sheet. Its characteristics allow it to fill a mould under the conditions of molding temperature and pressure employed. In our case, the SMC prepreg is made from glass strands chopped to lengths of 2.5 mm, sandwiched between two layers of film, onto which the resin paste has already been applied. The prepreg passes through a compaction system that ensures complete strand impregnation before being wound into rolls. These are stored for a few days before molding, to allow the prepreg to thicken to a moldable viscosity. Good mechanical and physical properties, together with some advantages in production, make SMC competitive with metals for automotive applications. As shown in Figure 1, the relatively low fibre volume fraction, which is in our case about 30%, and the uncontrolled filler and reinforcement distribution during processing lead to a more heterogeneous structure compared to the angle cross ply composites, with several kinds of stress concentrators such as glass fiber ends and interfaces, calcium carbonate filler and voids. The result is that, at quite an early stage, loading introduces various forms of local damages. The SMC samples are in the form of 120 mm barbell with 3 mm tickness. The $[\pm 62^o]$ and $[90^o/35^o]$ specimens are in parallelepiped form and have dimensions $14 \times 120 \times 2$ mm^3. All samples are cut using a diamond wheel saw to give a suitably smooth surface finish with the minimum sub-surface damage.

2.2 Mechanical testing

The creep tensile tests were performed using a servo-hydraulic mechanical testing system which is digitally controlled. The specimens were clamped with serrated wedge action grips. Special care was exercised while installing the grips to ensure alignment. Constant tensile load was applied to the specimens and the resulting strain was recorded. As the failure elongation of the polyester resin at room temperature is close to that of the glass fiber, the creep tensile tests were conducted at a higher temperature in order to have creep tests with substantial times to rupture for all specimens. After many exploratory creep tensile tests, we determined a range of temperatures T and stresses s giving manageable time to ruptures. Our results below have been obtained with $T = 60^o$C and $s = 15$ MPa for the $[\pm 62^o]_{12}$ specimens and with $T = 60^o$C and $s = 22$ MPa for the $[90^o/35^o]_{12}$ specimens. These temperatures are below the glass transition temperature of the resin which is 80^oC. The SMC specimens were loaded at $s = 48$ MPa at $T = 100^o$C. The stress is increased progressively and reaches a constant value after about 10 seconds (12 sec for $[\pm 62^o]_{12}$ specimens, 9 sec for $[90^o/35^o]_{12}$, and 17 sec for the SMC).

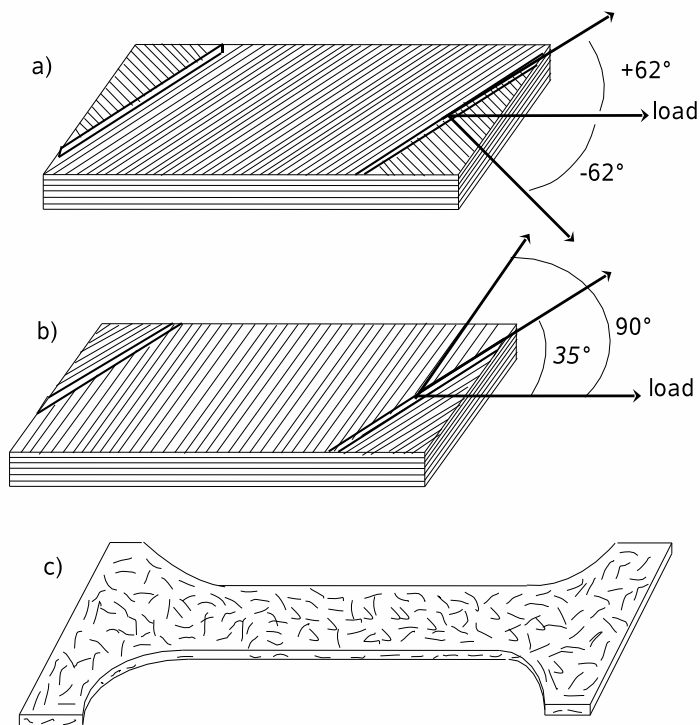Figure 1: Structure of Cross angle ply laminates (a) $[\pm 62^{o}]_{12}$ and (b) $[90^{o}/35^{o}]_{12}$ and (c) Sheet Molding Compound (SMC) composites.
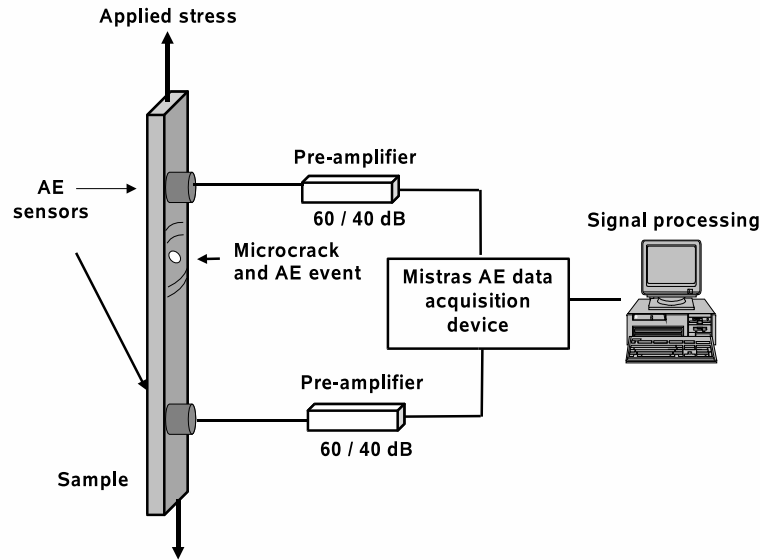
Figure 2: AE experimental device.

2.3 Acoustic emission testing

An external load applied to the composite materials considered in this study results in inhomogeneous stress and strain fields. The inhomogeneity of the stress field, coupled with the inhomogeneity of the strength and fracture properties of the reinforcing elements, the matrix, the interface and the fibers lead to a gradual development of damage. For such fiber-reinforced polymer composite laminates, failure results from the initiation and coalescence of damages of different types. The most typical damage mechanisms are matrix cracks, fiber matrix debounding, fiber breaks, and delaminations. Theoretical and experimental studies of these damage mechanisms in these composites are necessary to better understand their ultimate failure and lifetime. A number of nondestructive evaluation (NDE) techniques, such as thermography, eddy current, radiography, X-ray tomography, ultrasonics, can be used to analyse the damage evolution in composite materials. However, the characteristic sizes of the matrix cracks, fiber breaks, fiber-matrix disbonds, and ply-damage induced delaminations are usually too small to be detected individually by the conventional NDE techniques. Acoustic emission (AE) has been proposed to monitor real time damage in composites (Yamaguchi et al., 1991). In this method, ultrasonic waves generated by the rapid release of elastic energy during damage events are detected by piezoelectric sensors. The corresponding signal is amplified by a pre-amplifier and digitized by the AE system, as shown in Figure 2.
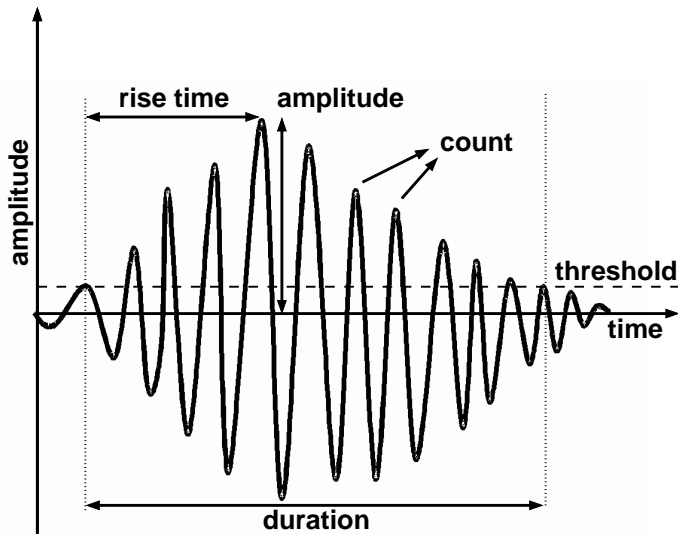
Figure 3: A typical acoustic emission signal.

Generally, the system can work in the parametric or in the transient mode. The parametric method is based on the extraction of a number of parameters from individual AE signals. A typical AE signal is shown in Figure 3. Some of the AE parameters are defined in this figure, including signal amplitude, duration, rise time, decay time, thresholds and AE counts.

Since the early works of Czochralski (1916), Portevin and Le Chatelier (1923), Förster and Scheill (1934), and Kaiser (1950), on metallic materials, AE analysis has been intensely used these last decades to characterize the overall damage accumulation in composites (Williams and Reifsnider, 1974; Beattie, 1983; Yamaguchi et al., 1991; Bakuckas et al., 1994, Ely and Hill, 1995; Luo et al., 1995; Shiwa et al. 1996). Williams and Reifsnider (1974) showed that the AE rate generally correlated with the rate of stiffness reduction due to damage. Numerous attempts to identify sources of the AE signals in composites have been made. Recently, Ono and Huang (1996), Prosser et al. (1995), Kloua et al. (1995), and de Groot et al. (1995) applied the transient waveform analysis for AE source recognition. Methods of pattern recognition analysis and neural networks were used for the AE signal classifications. It was shown for example by Huguet and al.(2002) for unidirectional glass fibre polymer composites that the wave shapes can be associated with particular damage mechanisms. These recent results showed that the transient AE analysis method based on the full waveform analysis may provide more powerful and robust capability to discriminate between the damage mechanisms.

A hybrid transient-parametric approach to separate overall AE histories into the histories for different damage micro-mechanisms in unidirectional composites was proposed by Dzenis and Qian (1998). The method was based on the combination of the transient AE waveform analysis and multiparameter filtering. The method was recently applied successfully to damage evolution analysis of cross-ply and angle-ply composites by Dzenis and Qian (2001).

In the present work, a two channel Mistras 2001 data acquisition system by Physical Acoustics Corporation was used for AE recording and analysis. The recorded AE amplitudes range from 0 dB to 100 dB. Two resonant sensors (200 kHz - 1 MHz) separated by 36 mm were put on the specimens using silicon grease as the coupling agent. Preliminary to recording during creep experiments, the data acquisition system has been calibrated for each sample by using a pencil lead break procedure (Nielsen,

1989). In this procedure, a reproducible acoustic wave is generated in the specimen by breaking a pencil lead on its surface. The lead breakage operation was repeated several times and at different locations between the sensors. The difference in arrival times on the sensors was deduced from the first peak of the signals they detected. From this information, the velocity and attenuation of the AE waves are determined simultaneously. After this calibration, the AE data acquisition was initiated simultaneously with the inception of mechanical loading. The acoustic emission was thus recorded from the beginning of the test all the way to the final failure of the specimen. The information on load and strain was continuously obtained from the mechanical testing and loading system. This information was stored in the parametric AE recording and allowed us to correlate the AE parameters with the load and strain at each time an AE signal was produced. Signal descriptors such as rise time, counts, energy, duration, amplitude and counts to peak were calculated by the software of the MISTRAS system. Furthermore, each waveform was digitized and stored. Using the transient analysis, other parameters were defined, such as the signal waveform, the average frequency, and so on. After storage and before processing, the signals were subjected to a linear location procedure to determine the location of the AE source. In the analysis of AE data, only events located between the sensors were used in order to reduce the acoustic noise generated by the testing machine and the grips.

We acknowledge that the complexity of wave propagation in composites increases the variability of AE signals. Multiple reflections from internal and external boundaries and the associated mode conversions interfere with the source wave and change the AE parameters that are detected. Despite this, AE can provide a meaningful and measurable response to some deformation and damage mechanisms and/or flow changes. Moreover, our aim in this paper is not to discriminate between the damage mechanisms but to record the overall damage accumulation. For this purpose, AE energy events and counts have shown their relevance (Anifrani et al., 1995; Garcimartin et al, 1997; El Guerjouma et al., 2001).

3 Creep damage and failure analysis

We recorded the strain and the acoustic signals (AE) emitted by microscopic failure events during the creep tests. Typical creep responses up to failure of the $[90^o/35^o]$ and $[\pm62^o]$ specimens are plotted in Figures 4 and 5 respectively with the associated AE activity shown as cumulated released energy and counts. Normal primary creep transients followed by secondary and tertiary creep were observed for almost all samples. Typical strain rate for both composites are shown in Figures 6, 7 and 8. Figure 8 shows the creep strain rate for the SMC composite #16.

These Figures show a rapid and continuous decrease of the strain rate in the primary creep regime, which can be described by Andrade's law

$$\frac{de}{dt} \sim \frac{1}{t^p} \, , \tag{1}$$

with an exponent p usually smaller than or equal to one (see the middle panels of Figures 6, 7 and 8 and Table 1). The crossover for small times is probably due to the fact that the stress does not reach immediately its constant value, but progressively increases up to about 10 sec after the start of the experiment.
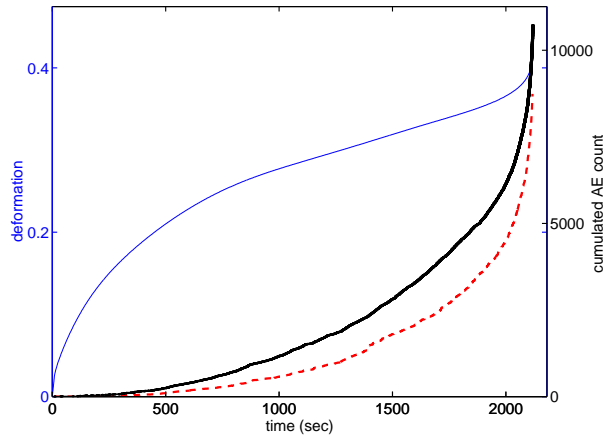
Figure 4: Creep strain and AE response for $[90^o/35^o]$ angle ply composite #3. The thin solid line is the deformation (left axis), the heavy black line is the cumulated AE count (right axis) and dashed line is the cumulated energy (arbitrary units).
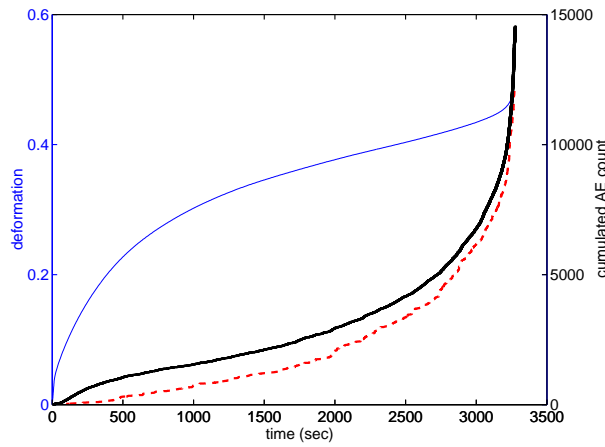

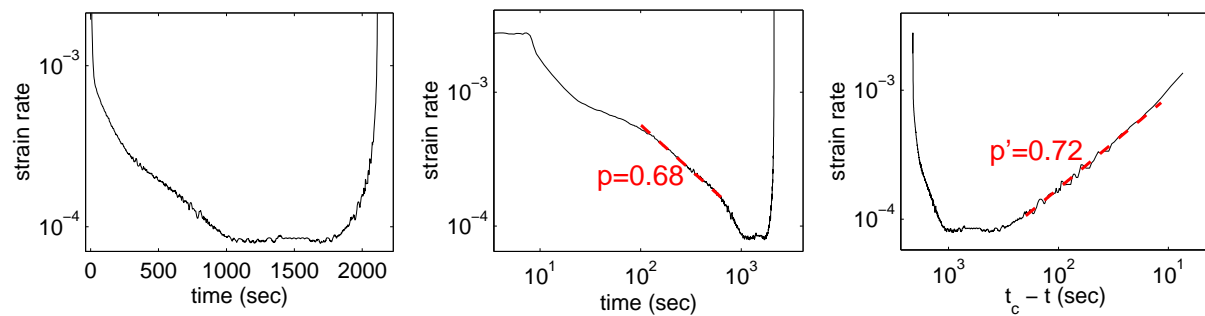Figure 5: Creep strain and AE response for $[\pm 62^o]$ angle ply composite #4. Same legend as in Figure 4.

Figure 6: Creep strain rate for $[90^o/35^o]$ angle ply composite #3. Left panel: full history in linear time scale; middle panel: time is shown in logarithmic scale to test for the existence of a power law relaxation regime; right panel: time is shown in the logarithm of the time to rupture time t_c such that a time-to-failure power law (2) is qualified as a straight line.
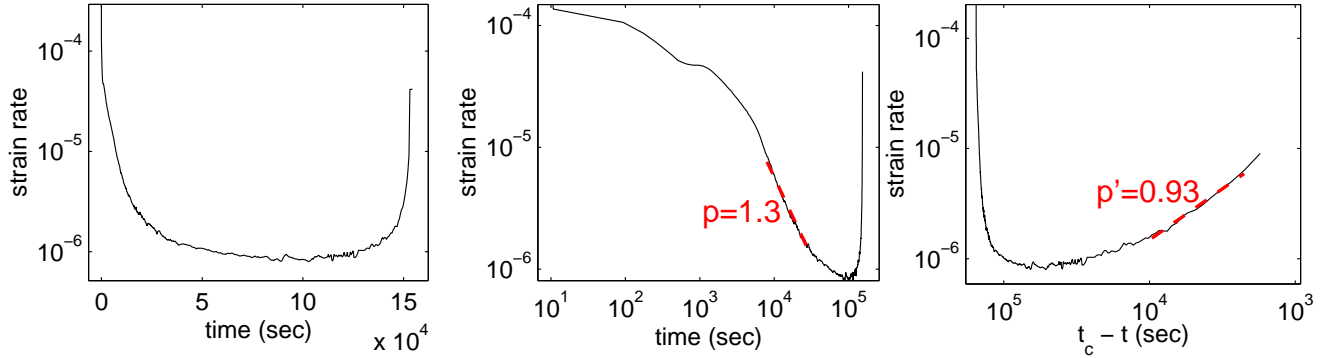
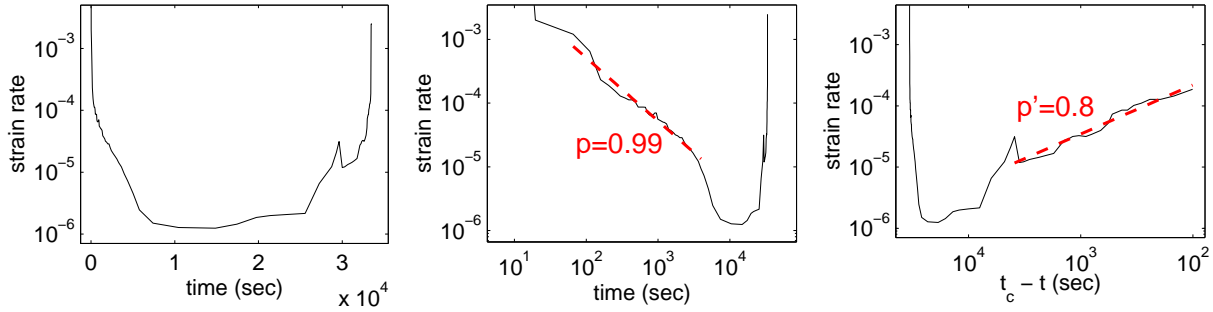Figure 7: Creep strain rate for $[\pm 62^o]$ angle ply composite #4. The three panels are as in figure 6.

Figure 8: Creep strain rate for SMC composite #16. The three panels are as in figure 6.

A quasi-constant strain rate (steady-state or secondary creep) is observed over an important part of the total creep time, and then followed by an increasing creep rate (tertiary creep regime) culminating in fracture. Creep strains at fracture point are large with values around 40% for angle cross ply composites and smaller (around 4%) for the SMC composites. The acceleration of the strain rate before failure is well fitted by a power-law singularity

$$\frac{de}{dt} \sim \frac{1}{(t_c - t)^{p'}} \; , \tag{2}$$

with an exponent $p' \leq 1$ (see the right panels of Figures 6 and 7 and Table 1). The critical time t_c determined from the fit of the data with expression (2) is generally close to the observed failure time (within a few seconds). The value of t_c in Table 1 and Figures 6 and 7 has been adjusted to obtain the best fit of the strain rate by equation (2).

   We obtain generally the same temporal evolution for the AE activity as for the strain rate, as shown in Figures 9, 10 and 11, except for the $[90^o/35^o]$ samples which do not display any decrease of the AE activity at early time while they present a clear relaxation of the strain rate. For $[90^o/35^o]$ samples, only one set of fibers is stressed (the 35° orientation). Therefore, the lack of AE activity for the $[90^o/35^o]$ samples may be due to the fact that the primary AE reflects a reorganization/relaxation between adjacent layers of different orientations. We also obtain the same pattern when plotting the AE event rate or the rate of AE energy. There are much larger fluctuations for the energy rate than for the event rate, due to the large distribution of AE energies, but the crossover time between primary creep and tertiary creep, and the values of p and p' are similar for the AE event rate and for the AE energy rate. This suggests that the amplitude distribution does not depend on time.

   The energy density distributions for all specimens ($[90^o/35^o]$, $[\pm 62^o]$ and SMC) are shown in Figure 12. The energy is measured by integrating the square of the amplitude of the signal over the duration of each event. All materials have similar energy distributions. The distributions of AE energies are
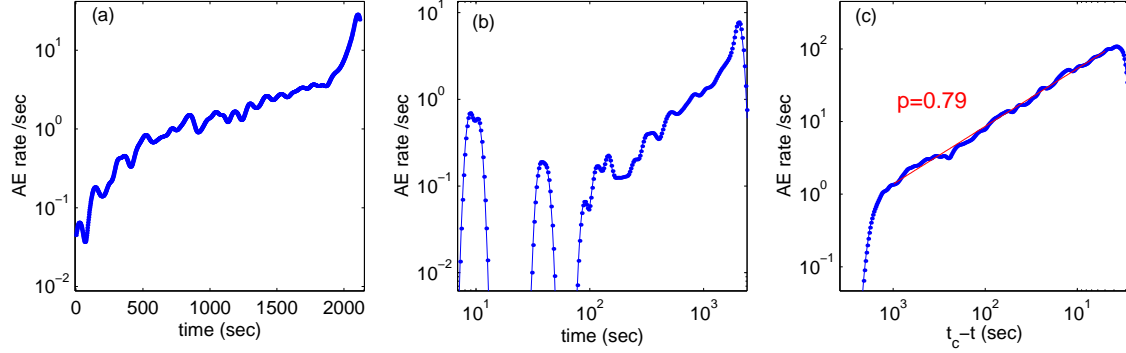
Figure 9: Rate of AE events for $[90^o/35^o]$ angle ply composite #3. Panel (a): full history in linear time scale; panel (b): time is shown in logarithmic scale to test for the existence of a power law relaxation regime (for this sample, this regime is not well-developed); panel (c): time is shown in the logarithm of the time to rupture time t_c such that a time-to-failure power law (2) is qualified as a straight line.
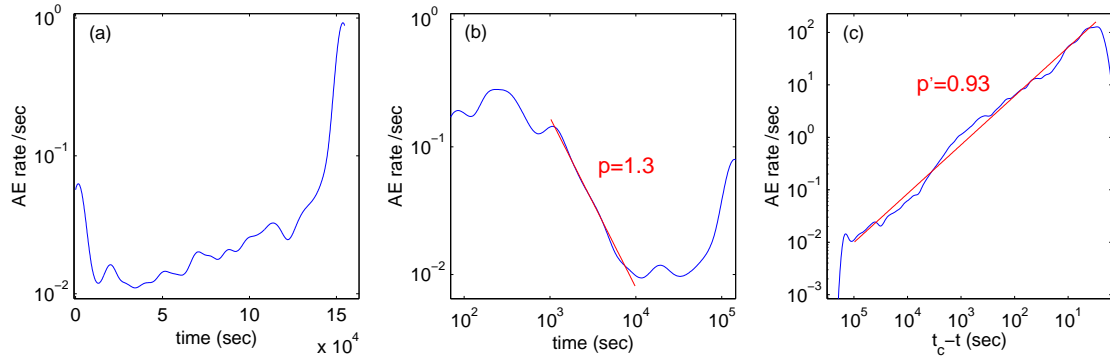

Figure 10: Rate of AE events for $[\pm 62^o]$ angle ply composite #4. The three panels are as in figure 9.
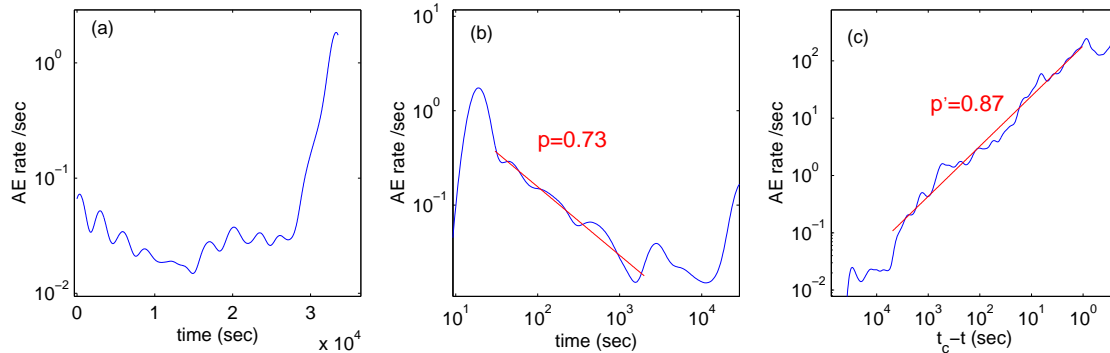

Figure 11: Rate of AE events for SMC composite #16. The three panels are as in figure 9.

Table 1: Strain rate: values of the critical time t_c, determined from the fit of de/dt by a power-law, the rupture time t_{end}, the transition time t_m between the primary and the tertiary creep regimes (determined as the time of the minimum of the strain rate), and the values of both exponents p defined in (1) and p' defined in (2). The time intervals used to estimate p and p' are given in column 3 and 5 respectively.

sample	p	$[t_{min} - t_{max}]$	p'	$[t_{min} - t_{max}]$	t_{end}	t_c	t_m
$[\pm 62^o]$ #1	0.84	500-3000	0.62	20-500	6617	t_{end}-12	4409
$[\pm 62^o]$ #2	0.79	700-8000	0.76	30-800	10214	t_{end}-3	7313
$[\pm 62^o]$ #3	0.99	400-2000	0.84	15-200	3267	t_{end}	2332
$[\pm 62^o]$ #4	1.30?	8000-30000	0.93	2000-10000	154398	t_{end}	95478
$[\pm 62^o]$ #5	0.91	500-5000	0.75	200-3000	8517	$t_{end} + 150$	4933
$[\pm 62^o]$ #6	0.97	500-3000	0.48	100-2500	6154	t_{end}	3436
$[\pm 62^o]$ #7	1.11	1500-7000	0.96	50-1000	13309	t_{end}	8313
$[90^o/35^o]$ #1	1.04	150-1100	0.81?	20-200	2307	t_{end}-40	1490
$[90^o/35^o]$ #2	0.27	20-300	0.45?	1-50	737	t_{end}-5	615
$[90^o/35^o]$ #3	0.68	100-700	0.72	10-200	2117	t_{end}	1214
smc #4	0.74	20-100	0.96	1-20	221	t_{end}-1.5	140.9
smc #6	0.92	25-150	1.03	0.5-80	339	t_{end}	186.5
smc #10	0.90	25-100	1.07	0.5-70	238	t_{end}	152.2
smc #11	0.87	25-400	0.69	1-100	686	t_{end}-2	411.8
smc #16	0.99	25-4000	0.85	100-4000	33539	t_{end}-30	14850.

'?' : large uncertainty on the values of the exponents, due to a limited range of times used in the fitting, or to large fluctuations of the strain rate, or because the results are very sensitive to the choice of t_c.

approximately power laws with an exponent of the pdf close to 1.5. This value is not far from the value ≈ 1.6 often found for earthquakes in subduction and transform zones (Kagan, 1999; Pisarenko and Sornette, 2003). The roll-off at small energies is due to the detection threshold. For the SMC and $[90^o/35^o]$ samples, there is a faster than power-law decay for large amplitudes. Figure 13 shows that the energy distribution does not depend on time. In particular the largest events do not occur preferentially close to failure but are also observed during primary creep, in contrast to one of the predictions of the critical point theory (Sornette and Vanneste, 1992; Johansen and Sornette, 2000).

We have also analyzed the one-dimensional location (along the long axis of the samples) of AE events. The AE events are rather uniformly distributed on the sample, and the spatial distribution is almost independent of time. In particular, we do not observe a significant or systematic localization of AE activity before failure.

Tables 1 (strain rates) and 2 (acoustic emissions) give the values of the critical time t_c, the transition time t_m between the primary and the tertiary creep regimes (determined as the position of the minimum of the strain rate), and the values of both exponents p defined in (1) and p' defined in (2).

There is a huge variability of the failure time from one sample to another one, for the same applied stress, as shown in Table 1. and in Figure 14. This implies that one cannot predict the time to failure of a sample using an empirical relation between the applied stress and the time of failure. There is however another approach suggested by Figure 14, which shows the correlation between the transition time t_m (minimum of the strain rate) and the rupture time $t_c \approx t_{end}$: t_m is found about 2/3 of the rupture time t_c. This suggests a way to predict the failure time from the observation of the strain rate during the primary and secondary creep regimes, before the acceleration of the damage during the tertiary creep
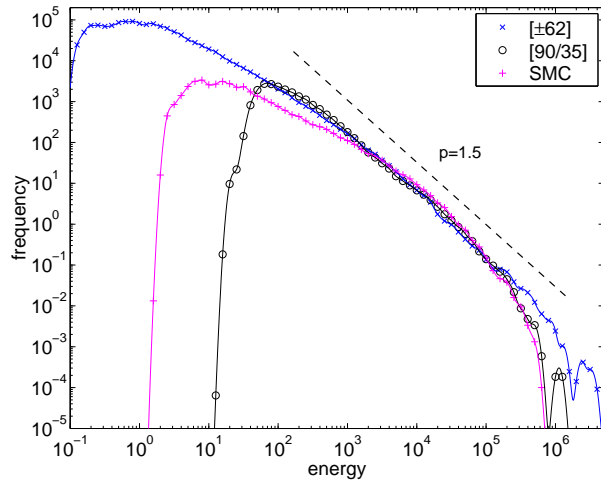
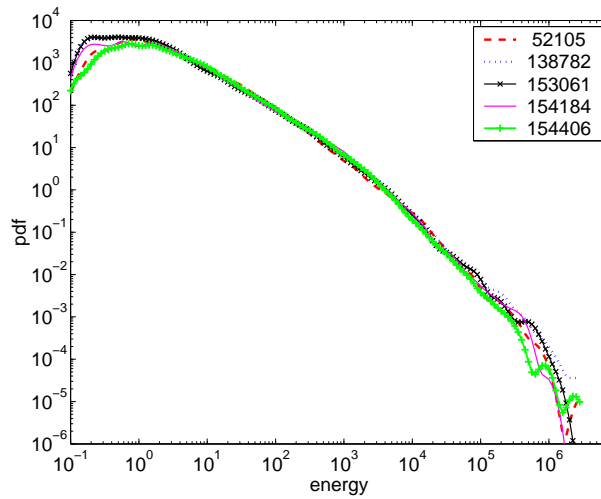Figure 12: Energy distribution for a $[90^o/35^o]$, a $[\pm 62^o]$ and a SMC specimen.

Figure 13: Energy distribution for the $[\pm 62^o]$ specimen #4 at different times, for 5 time windows with 3400 events each. The average time (in seconds) of events in each window is given in the caption.

Table 2: Acoustic emission rate: values of the critical time t_c, rupture time t_{end}, transition time t_m, and time intervals $[t_{min} - t_{max}]$ used to estimate p defined in (1) and p' defined in (2). N is the number of AE events.

sample	p	$[t_{min} - t_{max}]$	p'	$[t_{min} - t_{max}]$	t_{end}	t_c	N
$[\pm 62^o]$ #1	0.20	100-3000	0.37	1-3000	6624	t_{end}-9	5970
$[\pm 62^o]$ #2	0.57	100-3000	1.06?	1-300	10226	t_{end}-12	1074
$[\pm 62^o]$ #3	0.72	100-1000	0.91	10-3000	3273	t_{end}	1453
$[\pm 62^o]$ #4	1.30	1000-10000	0.93	3-100000	154799	t_{end}-400	17052
$[\pm 62^o]$ #5	0.41	100-3000	0.48	0.2-100	8518	t_{end}	11044
$[\pm 62^o]$ #6	0.37	100-3000	no tertiary creep		6083		1532
$[\pm 62^o]$ #7	0.47	500-8000	1.13?	1-100	13417	t_{end}-106	2826
$[90^o/35^o]$ #1	no primary creep		0.84	10-3000	2307	t_{end}-50	4014
$[90^o/35^o]$ #2	no primary creep		0.85	2-300	737	t_{end}	11383
$[90^o/35^o]$ #3	no primary creep		0.79	5-1000	2117	t_{end}+3	10724
smc #4	0.41?	20-120	0.87	1-50	221	t_{end}+0.5	1979
smc #6	1.05?	15-80	0.91	1-300	339	t_{end}	3406
smc #10	1.63?	15-80	1.10	2-100	238	t_{end}-1	3058
smc #11	0.77	25-500	0.94	4-100	688	t_{end}-25.1	546
smc #16	0.73	30-2000	0.87	1-5000	33539	t_{end}	7515

'?' : large uncertainty on the exponents values, due to a limited range of times used in the fitting, or to large fluctuations of the strain rate, or because the results are very sensitive to the choice of t_c.

regime leading to the rupture of the sample. As soon as a clear minimum is observed, the value of t_m can be measured and that of t_c deduced from the relationship shown in Figure 14. However, there are a few cases where the minima is not well defined, such as the one shown in Figure 6 for the $[90^o/35^o]$ angle ply composite #3 for which the first (smoothed) minimum is followed by a second similar one. In this case, the application of the relationship shown in Figure 14 would lead to a pessimistic prediction for the lifetime of the composite.

Figure 15 illustrates the correlations between different characteristics of the evolution of the strain rate and AE activity in the primary creep and before failure. There is no correlation between the p-value measured using the strain rate and the p-value of the AE rate (see Figure 15a). However, due to the rather large uncertainty on the p value (which is determined for a more limited time range than p', and for a smaller number of AE events), it is difficult to ascertain that the exponents p of the strain rate and of the AE data are different. A positive correlation is found for the exponent p' in the tertiary regime (see Figure 15b) measured for the strain rate and from the AE data. There is also a weak positive correlation between the exponent p and p' measured both for the strain rate (Figure 15c) or for the AE rate (Figure 15d). Finally, we observe a positive correlation between the Andrade exponent p and the rupture time, which is more significant for the strain rate than for the AE rate (Figure 15e). No such correlation is found between the rupture time and p' (Figure 15f).

The observation that the failure time is correlated with the p-value of the primary creep suggests that, either a single mechanism is responsible both for the decrease of the strain rate during primary creep and for the acceleration of the damage during the tertiary creep or, if the mechanisms are different nevertheless, the damage that occurs in the primary regime impacts on its subsequent evolution in the secondary and tertiary regime, and therefore on t_c. It also provides an additional way to predict the failure
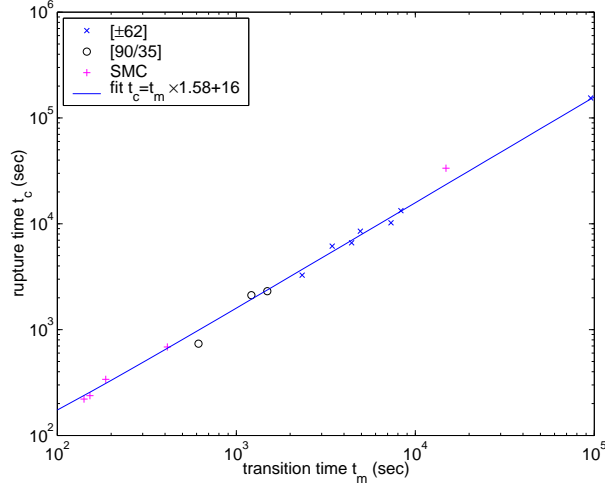
Figure 14: Relation between the time t_m of the minima of the strain rate and the rupture time t_c, for all samples (see table 1).
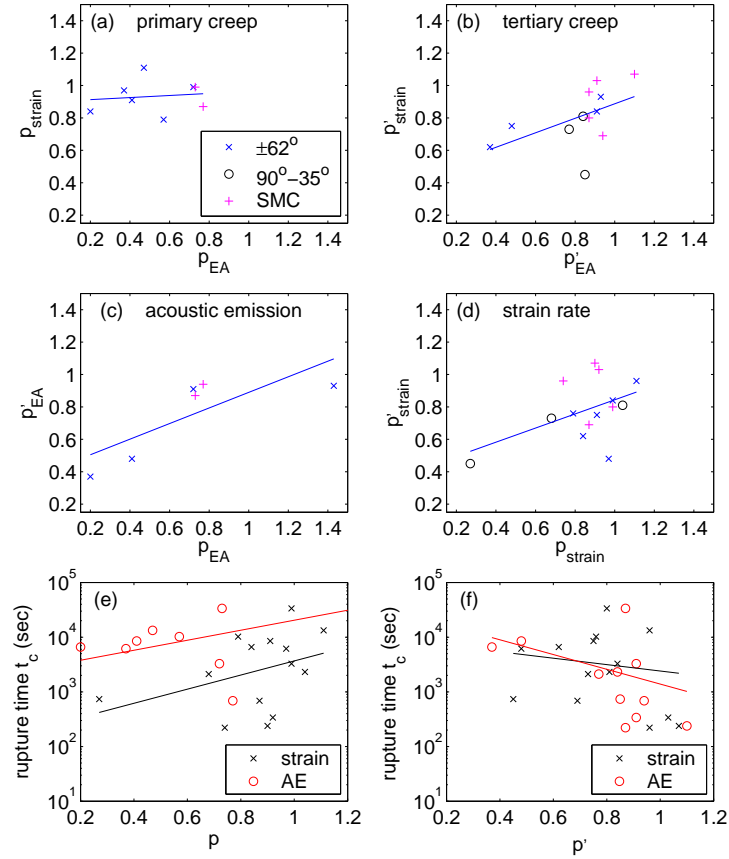

Figure 15: Correlation between different characteristics of the strain rate and acoustic emission data over all samples (see Tables 1 and 2). Symbols are data points (see legend in each panel) and solid lines are linear fits. We removed the data which are the more uncertain (noted '?' in Tables 1 and 2).

time from the observation of the strain rate or AE activity measured during the primary creep: the smaller the p-value, the shorter is the time before failure. A similar observation has been reported in Kuhn and Mitchell (1993). This correlation between the p-value and t_c comes as an additional information to the correlation between t_c and the time t_m at the minimum of the strain rate shown in Figure 14. Combining both correlations could help improve the prediction of the lifetime from the accurate recording of the primary regime and of its transition to the tertiary creep.

In contrast, using a fit of the AE activity by a power-law to estimate t_c according to formula (2) works only in the tertiary regime and thus does not exploit the information contained in the deformation and in the acoustic emissions of the primary and secondary regimes which cover 2/3 to 3/4 of the whole history. In practice, one needs at least one order of magnitude in the time $t_c - t$ to estimate accurately t_c and p', which means that, if the power-law acceleration regime starts immediately when the stress is applied (no primary creep), we cannot predict the rupture time using a fit of the damage rate by equation (2) before 90% of the failure time. If, as observed in the experiments, the tertiary creep regime starts only at about 63% of t_c, then we cannot predict the rupture time using a fit of the damage rate before 96% of the failure time. This limitation was one of the motivations for the development of formulas that extend the description of the acoustic emission rates beyond pure power laws and that interpolate between the primary and tertiary regimes (Johansen and Sornette, 2000; Moura and Yukalov, 2002; Yukalov et al, 2004). These work however do not impose a relation between the duration of the primary creep and the failure time which may be useful to predict t_c.

4 Model construction

4.1 Relation with previous works

Before presenting our model, we briefly discuss previous works that attempted to explain the power laws for the strain rates and/or acoustic emission rates observed in the primary and/or tertiary regimes. Vujosevic and Krajcinovic (1997), Turcotte et al. (2003), Shcherbakov and Turcotte (2003) and Pradhan and Chakrabarti (2004) use systems of elements or fibers within a probabilistic framework (corresponding to so-called annealed or thermal disorder) with a hazard rate function controlling the probability of rupture for a given fiber as a function of the stress applied to that fiber. Turcotte et al. (2003) obtain a finite-time singularity of the strain rate before failure in fiber bundle models by postulating a power law dependence of the hazard rate controlling the probability of rupture for a given fiber as a function of the stress applied to that fiber. Shcherbakov and Turcotte (2003) study the same model as Turcotte et al. (2003) and recover a power-law singularity of the strain rate for systems subjected to constant or increasing stresses with an exponent $p' = 4/3$ larger than our experimental results. Vujosevic and Krajcinovic (1997) also find this power-law acceleration in two-dimensional simulations of elements and in a mean-field democratic load sharing model, using a stochastic hazard rate, but they do not obtain Andrade's law in the primary creep regime. Shcherbakov and Turcotte (2003) obtain Andrade's law only in the situation of a system subjected to a constant applied strain (stable regime). But then, they do not have a global rupture and they do not obtain the critical power law preceding rupture. Thus, the models described above do not reproduce at the same time Andrade's law for the primary regime and a power-law singularity before failure.

The thermal fuse model (Sornette and Vanneste, 1992; Vanneste and Sornette, 1992) introduces a dynamical evolution law for the damage field in systems with long-range elastic interactions and frozen heterogeneities. It was initially formulated in the framework of electric breakdown. Sornette and Vanneste (1994) latter showed the equivalence of the thermal fuse-network with a (scalar) antiplane mechanical model of rupture with elastic interaction. In this model, the damage of each element is a function of the applied stress. Each element breaks when the damage reaches the rupture threshold. The global rupture

occurs as the culmination of the progressive nucleation, growth and fusion between microcracks, leading to a fractal network of micro-cracks. The total rate of damage, as measured for instance by the rate of elastic energy release, increases on average as $dE/dt \sim 1/(t_c - t)^{p'}$ before failure, with an exponent $p' \geq 1$ which depends on the damage law.

Miguel et al. (2002) reproduced Andrade's law with $p \approx 2/3$ in a numerical model of interacting dislocations, but their model does not reproduce the tertiary creep regime (no global failure).

Several creep models consider the democratic fiber bundle model (DFBM) with thermally activated failures of fibers. Pradhan and Chakrabarti (2004) consider the DFBM and add a probability of failure per unit time for each fiber which depends on the amplitude of a thermal noise and on the applied stress. They compute the failure time as a function of the applied stress and noise level but they do not discuss the temporal evolution of the strain rate. Ciliberto et al. (2001) and Politi et al. (2002) consider the DFBM in which a random fluctuating force is added on each fiber to mimic the effect of thermal fluctuations. Ciliberto et al. (2001) show that this model predicts a characteristic rupture time given by an Arrhenius law with an effective temperature renormalized (amplified) by the quenched disorder in the distribution of rupture thresholds. Saichev and Sornette (2003) show that this model predicts Andrade's law as well as a power law time-to-failure for the rate of fiber rupture with $p = p' = 1$, with logarithm corrections (which may give apparent exponents p and p' smaller than 1).

A few other models reproduce both a power-law relaxation in the primary creep and a finite time singularity in the tertiary regime. Main (2000) obtains a power-law relaxation (Andrade's law) followed by a power-law singularity of the strain rate before failure by superposing two processes of subcritical crack growth, with different parameters. A first mechanism with negative feedback dominates in the primary creep and the other mechanism with positive feedback give the power-law singularity close to failure. Lockner (1998) gives an empirical expression for the strain rate as a function of the applied stress in rocks, which reproduces, among other properties, Andrade's law with $p = 1$ in the primary regime and a finite-time singularity leading to rupture.

Kun et al. (2003) and Hidalgo et al. (2002) studied numerically and analytically a model of visco-elastic fibers, with deterministic dynamics and quenched disorder. They considered different ranges of interaction between fibers (local or democratic load sharing). Kun et al. (2003) derived the condition for global failure in the system and the evolution of the failure time as a function of the applied stress in the unstable regime, and analysed the statistics of inter-event times in numerical simulations of the model. Hidalgo et al. (2002) derived analytically the expression for the strain rate as a function of time. This model reproduces a power-law singularity of the strain rate before failure with $p' = 1/2$ in the case of a uniform distribution of strengths (Hidalgo et al., 2002) but is not able to explain Andrade's law for the primary creep. This model gives a power-law decay of the strain rate in the primary creep regime only if the stress is at the critical point, but with an exponent $p = 2$ larger than the experimental values.

Our model is inspired from the work of Kun et al. (2003) and Hidalgo et al. (2002). We progressively complexify their model to better account for the experimental observations and to identify the ingredients necessary to the observation of the power-law evolution of the strain rate in the primary and tertiary creep regimes.

4.2 Model 1: Representative elements with Kelvin rheology

4.2.1 Formulation of the model

We view a composite system as made of a large set of representative elements (RE), each element comprising many fibers with their interstitial matrix. Each RE is endowed with a visco-elasto-plastic rheology with parameters which may be different from one element to another. The parameters characterizing each RE are frozen and do not evolve with time (so-called quenched disorder). We assume that the applied load is shared democratically between all RE: each surviving RE is subjected to the same stress equal

to the total applied force divided by the number of surviving RE. This so-called mean-field formulation allows us to perform analytical calculations and thus to get a better qualitative understanding of the physics. This simplifying assumption has been shown to be a good approximation of the elastic load sharing for sufficiently heterogeneous materials (Roux and Hild, 2002; Reurings and Alava, 2004).

Each RE is modeled as a dashpot of viscous coefficient b put in parallel with a purely elastic element of elastic constant E, that is, each RE has a Kelvin rheology. Applied to our experiments, this would correspond to a fiber-matrix composite made of long fibers embedded in a visco-elastic matrix which run all the way through the sample from one extremity to the other. A given RE is assumed to fail when its elongation/deformation e reaches a threshold. The rupture thresholds are distributed according to a cumulative distribution $P(e)$, giving the number of thresholds smaller than e. A rupture threshold is uniquely assigned to a given RE and remains constant throughout the deformation. This first model has been introduced in the language of the democratic fiber bundle model (DFBM) extended to allow for the presence of creep (Kun et al., 2003; Hidalgo et al., 2002), with different choices of rupture thresholds.

We assume that the fraction of broken RE is governed by

$$P(e) = 1 - \left(\frac{e_{01}}{e + e_{02}} \right)^{\mu} , \tag{3}$$

where e_{01} and e_{02} are two constants with $e_{01} \leq e_{02}$. The fraction $1 - (e_{01}/e_{02})^{\mu}$ breaks as soon as the stress is applied, in agreement with experiments which show that acoustic emission starts immediately when the stress is applied. The power-law distribution of rupture thresholds for large e is suggested by the large distribution of failure times for the same applied stress (see Figure 14). The exponent $\mu > 0$ controls the amplitude of the frozen heterogeneity of the RE strengths. The larger μ is, the less heterogeneous is the system. We shall consider that μ is in general larger than 1 so that the average strength of a RE has a meaning but μ may be smaller than 2 for which the variance of the fiber strength is not defined.

The initial stress per RE, before any damage has occurred, is equal to the applied load s. The equation controlling the deformation $e(t)$ in each surviving RE as a function of time is

$$b\frac{de}{dt} + Ee = \frac{s}{1 - P(e)} = s \left(\frac{e + e_{02}}{e_{01}} \right)^{\mu} , \tag{4}$$

with the initial condition $e(t = 0) = 0$. The right-hand-side of this equation gives the stress per remaining RE when the deformation (of both the elastic and anelastic parts) is e. $1 - P(e)$ is the fraction of unbroken RE. By construction of the model, the RE are associated in parallel and they all have the same deformation e obeying the same equation (4). The left-hand-side of (4) expresses the stress within a RE as being shared between the dashpot and the elastic element in the Kelvin rheology.

4.2.2 Condition for global failure

The system defined by (4) has a stable and an unstable regime as a function of the applied stress s. The system is stable if the differential equation (4) has a stationary solution $de/dt = 0$ with $e > 0$, i.e. if the following equation has a non-trivial solution:

$$\left(\frac{e + e_{02}}{e_{01}} \right)^{\mu} = \frac{E}{s} e . \tag{5}$$

For small s, the differential equation evolves toward a constant deformation e given by the smallest of the two solutions of (5) which is stable, as shown in Figure 16. There is a threshold s^* above which eq. (5) does not have a solution and $\frac{de}{dt}$ grows without bound leading to the global failure of the system.
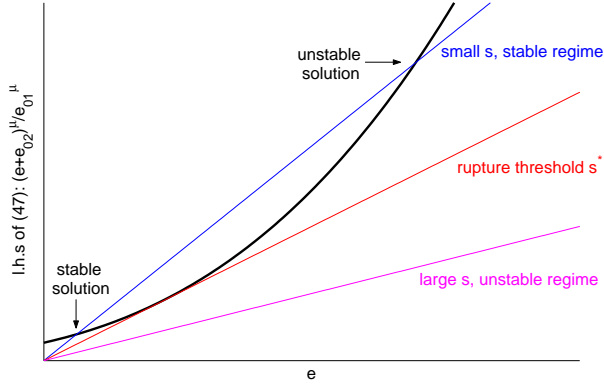
Figure 16: The thick curve is the left-hand-side of condition (5) as a function of e. The three thin straight lines are the right-hand-side $\frac{E}{s}e$ of (5) for three values of the applied stress s. The rupture of the system occurs for sufficiently large stress s for which condition (5) does not have a solution.

4.2.3 Properties of the model

At short times for which the deformation is small, we have $e \ll e_{02}$. In this regime $(e + e_{02})^\mu \approx e_{02}^\mu(1 + \mu e/e_{02})$. We can thus rewrite (4) as

$$ b\frac{de}{dt} + Ee = s \left(\frac{e_{02}}{e_{01}}\right)^\mu \left(1 + \mu\frac{e}{e_{02}}\right) , \tag{6}$$

whose solution is (with initial condition $e(0) = 0$)

$$ \frac{de}{dt} = \frac{s}{b} \left(\frac{e_{02}}{e_{01}}\right)^\mu e^{-t\left(\frac{E}{b} - \frac{s\mu}{be_{02}}\left(\frac{e_{02}}{e_{01}}\right)^\mu\right)} . \tag{7}$$

After a jump at $t = 0$, the deformation rate decays exponentially with time if the stress is small, or starts to accelerate at $t = 0$ without a primary creep regime if the stress or e_{02}/e_{01} are large enough so that the term in the exponential of (7) is positive.

In the unstable regime $s > s^*$, the deformation rate accelerates before failure. Close to failure, we have $e \gg e_{02}$ and we can rewrite (4) as

$$ b\frac{de}{dt} + Ee = s \left(\frac{e}{e_{01}}\right)^\mu . \tag{8}$$

As the deformation increases, eventually the term in the right-hand-side of (8) dominates over Ee, which yields the asymptotic equation

$$ b\frac{de}{dt} = s \left(\frac{e}{e_{01}}\right)^\mu . \tag{9}$$

Its solution is

$$ e(t) \approx \left(\frac{be_{01}^\mu}{s(\mu - 1)}\right)^m \frac{1}{(t_c - t)^m} , \quad \text{where } m = 1/(\mu - 1) . \tag{10}$$

The cascades of RE ruptures give rise to a finite-time singularity, i.e., the deformation diverges in finite time. The critical time t_c is fixed by matching this asymptotic regime (9) with the short-time solution (7). Of course, in reality, there are no divergences in a system of finite size. This solution only expresses a very fast acceleration of the deformation leading to a failure of the system in finite time at or very close to t_c. The deformation rate is thus proportional to

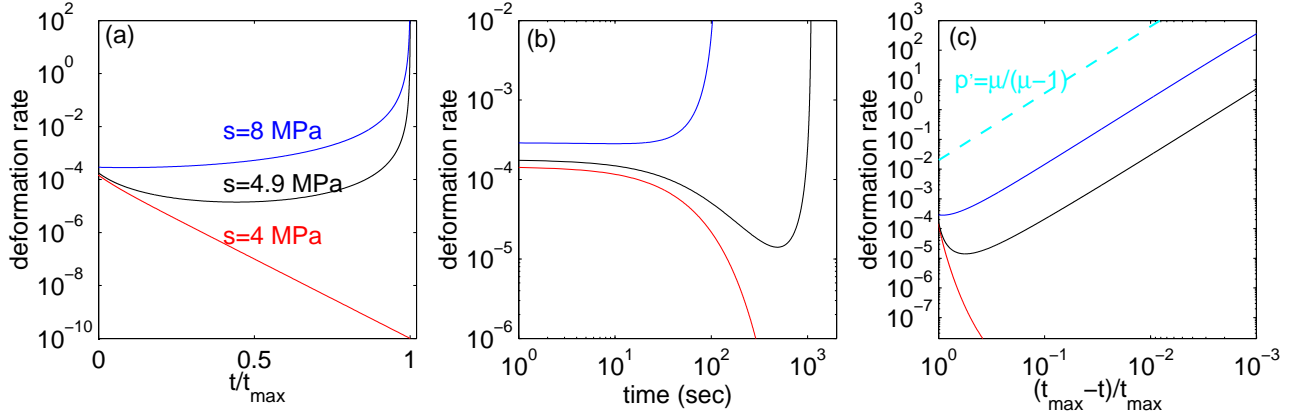$$ \frac{de}{dt} \sim \frac{1}{(t_c - t)^{\mu/(\mu - 1)}} . \tag{11}$$

Figure 17: Strain rate de/dt estimated by the numerical solution of eq. (4) for different values of the stress s, and with parameters $E = 20$ GPa, $\mu = 1.8$, $e_{01} = 0.003$, $e_{02} = 0.015$, $b = 5 \times 10^{11}$ Pa.sec. Panel (b) illustrates the absence of Andrade's law in the primary regime. Panel (c) illustrates the power law acceleration of the strain rate before failure for $s = 4.9$ MPa and $s = 8$ MPa with an exponent asymptotically equal to $p' = \mu/(\mu - 1) = 2.25$ (dashed line). The time t_{max} used to normalize the curves in (a) and (c) is the rupture time (for $s = 4.9$ MPa and $s = 9$ MPa) or the time when de/dt decreases below 10^{-14} (numerical accuracy) for $s = 4$ MPa.

Since $\mu > 1$, the exponent $p' = \mu/(\mu - 1)$ is larger than 1, in contradiction with the experimental results shown in Tables 1 and 2.

Figure 17 shows the numerical solution of the differential equation (4) for different values of the stress, which are in good agreement with the approximate solutions (7) for the primary creep and (11) close to failure.

Our experiments record not only the deformation rate de/dt but also the rate of acoustic emissions (number of counts per unit time) radiated by the sample. If we assume that the rate of acoustic emissions is proportional to the failure rate of RE, the acoustic emission rate close to failure is given by

$$\frac{dN}{dt} = \frac{dP}{de}\frac{de}{dt} \sim \frac{1}{(t_c - t)^{1-m\mu}} \sim (t_c - t)^{1/(\mu-1)} \,, \tag{12}$$

where we have used (10) to get the last expression on the right. Thus, rather than increasing in the final stage of deformation as often observed experimentally, the acoustic emission count rate goes to zero according to Model 1. Experimentally, we have observed the same temporal evolution for the strain rate de/dt and for the AE rate dN/dt, in disagreement with the result (12). This simple model may be inadequate to reproduce AE data. In contrast with the DFBM model (network of elastic fibers loaded with increasing stress), there is no avalanches in this model: the rupture of one element does not immediately trigger the rupture of other elements (Kun et al., 2003). Therefore in our further modelling work we will focus on the analysis of the strain rate.

In conclusion, while Model 1 exhibits some of the qualitative properties reported in our experiments (initial decay of the deformation rate and power law acceleration of the deformation rate leading to rupture), it fails to reproduce Andrade's law for the initial decay (exponential versus power law) and the observation that the exponent p' of the critical acceleration of the deformation rate is smaller than 1. Note that this model with a uniform distribution of failure thresholds gives an exponential relaxation for $s \neq s^*$ and the power law $de/dt \sim 1/t^2$ only for the critical value $s = s^*$ (Hidalgo et al., 2002).

4.3 Model 2: Power-law shear-thinning creep with Kelvin fibers

Let us therefore consider the following modification of the model. Rather than taking a Newtonian viscous dashpot, we propose to consider a dashpot with shear-thinning rheology (Astarita and Marrucci, 1974) which consists in replacing b by $b_0|de/dt|^{n-1}$, with $n < 1$. This shear-thinning power law rheology represents at the mesoscopic RE level the fiber-matrix interaction which involves micro-cracking and delamination. The governing equation replacing expression (4) reads

$$b_0|de/dt|^{n-1}\frac{de}{dt} + Ee = \frac{s}{1 - P(e)} \ . \tag{13}$$

At short times when $e \ll e_{02}$, expression (13) reduces to

$$b_0|de/dt|^{n-1}\frac{de}{dt} + Ee = s\ \left(\frac{e_{02}}{e_{01}}\right)^{\mu}\ (1 + \mu\frac{e}{e_{02}}) \tag{14}$$

whose solution for the strain rate is

$$\frac{de}{dt} = \frac{(e_{02}bng)^{1/(1-n)}}{[e_{02}bn + tg(1 - n)(Ee_{02} - sf\mu)]^{1/(1-n)}} \tag{15}$$

where the constants f and g are defined by

$$f = \left(\frac{e_{02}}{e_{01}}\right)^{\mu} \tag{16}$$

$$g = \left(\frac{sf}{b}\right)^{(1-n)/n} \tag{17}$$

Expression (15) describes a constant strain rate at times smaller than t^* given by

$$t^* = \frac{e_{02}bn}{g(1 - n)(Ee_{02} - sf\mu)} \tag{18}$$

followed by a power law decrease $\sim 1/t^p$ at times $t \gg t^*$ with an exponent $p = 1/(1 - n)$ larger than one if $n < 1$.

Note that the exponent p does not depend on the exponent of the distribution of rupture thresholds. Changing the distribution of rupture thresholds, e.g. by taking an exponential distribution or assuming that there is no rupture of RE for $e < e_{01}$, does not change qualitatively the behavior of the strain rate in the primary creep regime. It only changes the crossover time t^* and the amplitude of the strain rate. This expression for a power-law rheology with shear-thinning rheology improves on the exponential relaxation (7) but predicts an exponent p still larger than 1.

At larger times and for $s > s^*$, the strain rate accelerates up to failure. When $e \gg e_{02}$, the equation governing the evolution of e becomes

$$b_0|de/dt|^{n-1}\frac{de}{dt} + Ee = s\ \left(\frac{e}{e_{01}}\right)^{\mu}\ . \tag{19}$$

As with (8), when the deformation increases, eventually the term in the right-hand-side of (19) dominates over Ee, which leads to the asymptotic equation

$$b_0|de/dt|^{n-1}\frac{de}{dt} \approx s\ \left(\frac{e}{e_{01}}\right)^{\mu}\ , \tag{20}$$
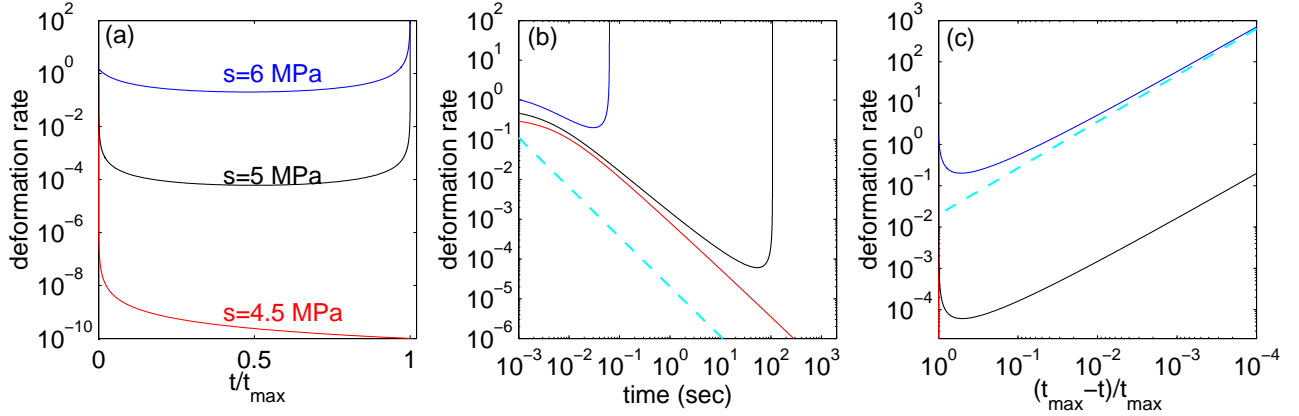
Figure 18: Strain rate de/dt estimated by the numerical solution of eq. (13) for different values of the stress s, and with parameters $E = 20$ GPa, $\mu = 1.8$, $n = 0.2$, $e_{01} = 0.003$, $e_{02} = 0.015$, $b = 1 \times 10^8$ Pa.sec^n. Panel (b) illustrates Andrade's law in the primary regime with an exponent close to the prediction $p = 1/(1-n) = 1.25$ (dashed line). Panel (c) illustrates the power law acceleration of the strain rate before failure for $s = 5$ MPa and $s = 6$ MPa with an exponent asymptotically equal to $p' = (\mu/n)/[(\mu/n) - 1] = 1.125$ (dashed line). The time t_{max} used to normalize the curves in (a) and (c) is the rupture time (for $s = 5$ MPa and $s = 6$ MPa) or the time when de/dt decreases below 10^{-14} (numerical accuracy) for $s = 4.5$ MPa.

whose solution for de/dt reads

$$\frac{de}{dt} \sim \frac{1}{(t_c - t)^{p'}}, \quad \text{where } p' = \frac{\mu/n}{(\mu/n) - 1} . \tag{21}$$

The deformation rate has a power-law singularity with an exponent p' larger than 1.

Figure 18 shows the numerical solution of the differential equation (13) for different values of the stress, which are in good agreement with the approximate solutions (15) for the primary creep and (21) close to failure.

The shear-thinning power law rheology for the dashpot with the Kelvin topology captures the main properties of the experiments, the power-law evolution of the strain rate in the primary and tertiary creep regimes. However the quantitative values of p and p' are larger than one in the model, in disagreement with the values measured in our experiments.

4.4 Model 3: Eyring rheology

We propose here another model which consist of an Eyring dashpot in parallel with a linear spring of stiffness E. The Eyring rheology (22) is standard for fiber composites (Agbossou et al., 1995; Liu and Ross, 1996). It consists, at the microscopic level, in adapting to the matrix rheology the theory of reaction rates describing processes activated by crossing potential barriers.

The deformation e of the Eyring dashpot is now governed by

$$\frac{de}{dt} = K \sinh(\beta s_1) . \tag{22}$$

where the stress s_1 in the dashpot is given as previously by $s_1 = s/(1 - P(e)) - Ee$.

Using the same distribution of rupture threshold $P(e)$ as previously, the differential equation for e (with initial condition $e(0) = 0$) is thus

$$\frac{de}{dt} = K \sinh\left(\frac{\beta s}{e_{01}{}^\mu}(e + e_{02})^\mu - \beta E e\right) . \tag{23}$$

Let us give the approximative solution of the deformation in the primary creep regime for $\beta s_1 \gg 1$ and $e \ll e_{02}$. In this regime, we have $\sinh(\beta s_1) \approx \exp(\beta s_1)/2$ and $(e + e_{02})^\mu \approx e_{02}{}^\mu(1 + \mu e/e_{02})$. We can thus rewrite (23) as

$$\frac{de}{dt} \approx \frac{K}{2} \exp\left(\frac{\beta s e_{02}{}^\mu}{e_{01}{}^\mu}(1 + \mu\frac{e}{e_{02}}) - \beta E e\right) , \tag{24}$$

which has the solution

$$\frac{de}{dt} = \frac{K e_{02}}{2 e_{02} \exp\left(-\beta s \left(\frac{e_{02}}{e_{01}}\right)^\mu\right) + t K \beta \left(E e_{02} - \mu s \left(\frac{e_{02}}{e_{01}}\right)^\mu\right)} . \tag{25}$$

Expression (25) predicts that, if the stress is not too large so that the term in the exponential of (24) is negative, de/dt is of the Andrade form $\sim t^{-p}$, with an exponent $p = 1$ at early times. For larger s, the strain rate starts to accelerate when the load is applied. Note that the observation of Andrade's power-law creep in this model, as for the previous models, is not dependent on the choice of the distribution of rupture thresholds $P(e)$. We obtain for instance the same behavior $de/dt \sim 1/(t + c)$ if we take $P(e) = 0$ for all e (no broken RE).

An approximate analytical solution of (23) in the tertiary creep is obtained by neglecting e_{02} compared with e. Close to failure, for large e, the linear term Ee is small compared with $s_2 = \frac{s}{e_{01}{}^\mu}(e + e_{02})^\mu$ if $\mu > 1$. This leads to the equation

$$\frac{de}{dt} \approx \frac{K}{2} \exp\left(\frac{\beta s e^\mu}{e_{01}{}^\mu}\right) . \tag{26}$$

Its solution is to leading logarithmic order (to be defined just below)

$$e(t) = A \left[-\ln(t_c - t)\right]^{\frac{1}{\mu}} , \tag{27}$$

$$\frac{de}{dt} = \frac{A}{\mu} \left[-\ln(t_c - t)\right]^{\frac{1}{\mu}-1} \frac{1}{t_c - t} , \tag{28}$$

where A is given by

$$A = e_{01} (\beta s)^{-1/\mu} . \tag{29}$$

The solutions (27) and (28) are correct up to $\ln(\ln(t_c - t))$ correction terms for $e(t)$ and up to $\ln(t_c - t)$ terms for $\frac{de}{dt}$. This means that only the leading power law $1/(t_c - t)$ is obtained reliably in the self-consistent solution (28), while logarithm corrections are not determined. The solutions (25) and (28) are of the same form with $p = p' = 1$ as the Langevin-type model solved by Saichev and Sornette (2003). This may not be surprising since the Eyring rheology describes, at the microscopic level, processes activated by crossing potential barriers, which are explicitly accounted for in the thermal fluctuation force model (Saichev and Sornette, 2003).

Expression (23) shows, similarly to the discussion in section 4.2.2 on the Condition for global failure for model 1 with equation (5), that rupture will occur only if the argument $B \equiv \frac{\beta s}{e_{01}{}^\mu}(e + e_{02})^\mu - \beta E e$ of the sinh in expression (23) never vanishes for any value of $e > 0$. If the stress is smaller than the threshold s^*, the equation $B = 0$ has two solutions and the system does not fail. If $s > s^*$, B does not vanish and the system fails in finite time. If s is close to but larger than s^*, B can be expanded as follows around its minimum:

$$B = c_1(s - s^*) + c_2(e - e^*(s))^2 , \tag{30}$$

where $e^*(s)$ is the value of the deformation which makes B minimum and c_1 and c_2 are two positive constants. Since $s \to s^*$ from above, $s - s^*$ is small. Also, the lifetime of the system is controlled by the domain of deformation giving the smaller strain rate, that is, for deformations e in the neighborhood of $e^*(s)$. We can thus expand $\sinh(B) \approx B$ to linear order and still obtain the correct scaling of the total lifetime. This leads to approximate equation (23) by

$$\frac{de}{dt} = K \left[c_1 (s - s^*) + c_2 (e - e^*(s))^2 \right] . \tag{31}$$

The change of variable $t \to \tau = t \, (s - s^*)^{1/2}$ and $e \to x = e \, (s - s^*)^{-1/2}$ transforms (31) into

$$\frac{dx}{d\tau} = K \left[c_1 + c_2 (x - x^*(s))^2 \right] . \tag{32}$$

The lifetime τ_c is obtained as

$$\tau_c \approx \int_0^{+\infty} dx \, \frac{1}{(dx/d\tau)} \tag{33}$$

which is a pure number independent of s. This thus gives $t_c \, (s - s^*)^{1/2} = \tau_c$ and thus

$$t_c \sim 1/(s - s^*)^{1/2} . \tag{34}$$

This result (34) holds also for model 1 (Hidalgo et al., 2002; Kun et al., 2003), as it is based solely on the expansion (30) and its analogs for model 1, which is generic. This universality expresses only the topology of a straight line almost tangent to a smooth curve similar to that shown in Figure 16, such that the distance of the curve to the straight line is given by an expression such as (30). For model 2, the dependence (34) is modified due to the nonlinear shear-thinning rheology. In this case, expression (31) is changed into

$$\left(\frac{de}{dt} \right)^n \sim \left[c_1 (s - s^*) + c_2 (e - e^*(s))^2 \right] . \tag{35}$$

The change of variable $t \to \tau = t \, (s - s^*)^{-\frac{1}{2} + \frac{1}{n}}$ and $e \to x = e \, (s - s^*)^{-1/2}$ transforms (35) into a non-dimensional equation. This transformation predicts $t_c \sim 1/(s - s^*)^{\frac{1}{n} - \frac{1}{2}}$ for model 2, which is verified by our direct numerical integration.

The dependence of t_c as a function of s for $s \gg s^*$ can also be predicted analytically as follows. Since the time-to-failure t_c is controlled by the primary and secondary regimes which last significantly longer than the final accelerating tertiary regime, the dependence of t_c on s is simply obtained from the dependence of the duration of the primary regime on s. This dependence is obtained by rewriting equation (24) as

$$\frac{de}{dy} \approx e^{\alpha e} , \tag{36}$$

where

$$\alpha = \frac{\beta s e_{02}{}^\mu}{e_{01}{}^\mu} \frac{\mu}{e_{02}} - \beta E , \tag{37}$$

and

$$y \equiv t \, \frac{K}{2} \, e^{\gamma s} . \tag{38}$$

with

$$\gamma = \frac{\beta e_{02}{}^\mu}{e_{01}{}^\mu} . \tag{39}$$

With the reduced time y, expression (36) is now dimensionless. Thus, the duration of this regime and thus t_c scale as

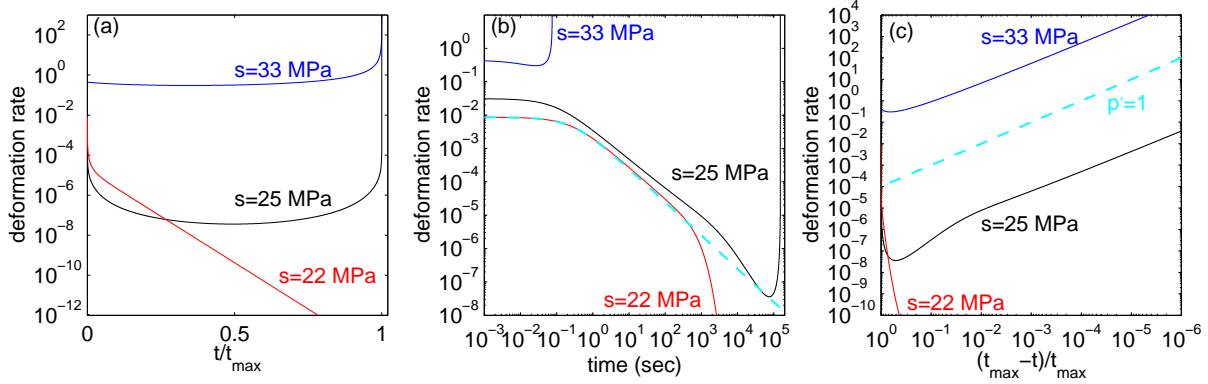$$t_c \sim \exp(-\gamma s) . \tag{40}$$

Figure 19: Strain rate de/dt estimated by the numerical solution of eq. (23) for different values of the stress s, and with parameters $E = 20$ GPa, $\mu = 1.2$, $e_{01} = 0.003$, $e_{02} = 0.015$, $\beta = 50$ GPa^{-1} and $K = 10^{-5}$ sec^{-1}. Panel (b) illustrates Andrade's law in the primary regime, with exponent $p \approx 1$ for $s = 22$ MPa and $p \approx 0.8$ for $s = 25$ MPa. Panel (c) illustrates the power law acceleration of the strain rate before failure for $s = 25$ MPa and $s = 33$ MPa with an exponent equal to 1 asymptotically but slightly smaller than one in the crossover further from rupture. The time t_{max} used to normalize the curves in (a) and (c) is the rupture time ($de/dt > 10^{20}$) for $s = 25$ MPa and for $s = 33$ MPa, and is defined by the time when de/dt decreases below 10^{-14} (numerical accuracy) for $s = 22$ MPa. The dashed line in (b) is the approximate solution (25) of (23) with $s = 22$ MPa for the primary creep (power-law with $p = 1$ at large t).

The predictions (34) and (40) for $t_c(s)$ are verified in Figure 20. Contrary to the primary regime, the heterogeneity of the rupture threshold is an essential ingredient for the observation of a power-law singularity. The acceleration toward failure is due to the positive feedback effect of broken RE, which increases the stress and deformation on the unbroken RE leading to the global failure of the system. We can observe the same power-law singularity (but only on a finite range of times) if we replace the power-law distribution of rupture threshold by an exponential distribution $P(e) = 1 - \exp(-e/e_0)$ with a large enough heterogeneity e_0. As long as the strain e is small compared to e_0, we have $P(e) \approx e/e_0$, therefore the stress s_1 in the dashpot is proportional to e leading to $de/dt \sim 1/(t_c - t)^{p'}$ close to failure.

Figure 19 shows the numerical solution of the differential equation (23) together with the approximate analytical solutions (25) in the primary creep and (28) close to failure, for different values of the applied stress s. In contrast with the analytical solution (25) for the primary creep, which predicts $p = 1$, we observe close to the rupture threshold $s \approx s^*$ an apparent smaller exponent $p \approx 0.8$ over 2 orders of magnitude in time, which can explain the values of $p < 1$ found experimentally (see Table 1). For a stress s much larger than s^*, the strain rate de/dt accelerates immediately when the load is applied. For $s < s^*$, there is an exponential decrease of the strain rate de/dt after the Andrade regime (see Figure 19). Close to failure for $t \approx t_c$ and $s > s^*$, the numerical integration of (23) shows that $\frac{de}{dt} \sim 1/(t_c - t)$ (26) is a good approximation very close to failure, but that for $s \approx s^*$ we can observe a crossover further from failure with an apparent exponent $p' = 0.9$. The numerical integration of (23) shows that both power-laws in the primary and tertiary creep regimes are obtained in this model, with an apparent exponent p for the primary creep smaller than 1, and with an exponent $p' = 1$ for the tertiary regime, except from a crossover with an apparent exponent p' a little smaller than one. This crossover with $p' < 1$ is not sufficient to explain the observations of $p' \approx 0.8$ over 4 orders of magnitude in time $t_c - t$.

Figure 20 shows the failure time t_c as a function of the applied stress. The failure time has a power-law singularity $\sim (s - s^*)^{-1/2}$ for $s \approx s^*$, as found previously by Hidalgo et al. (2002) and Kun et al. (2003) for the first version of the model (linear dashpot). The failure time decays exponentially for
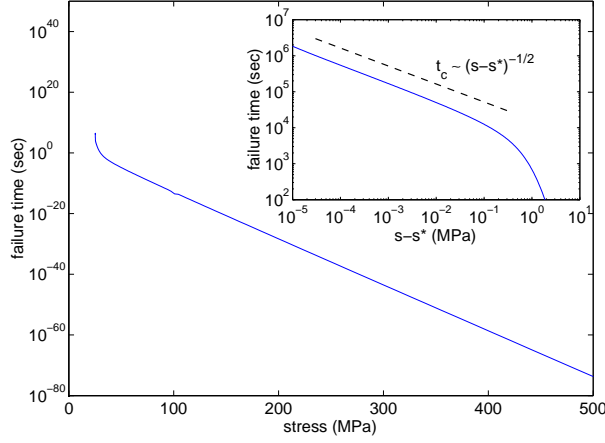
Figure 20: Lifetime t_c as a function of the applied stress s, for the same parameters as in Figure 19. The failure time decreases exponentially with s for $s \gg s^*$ and decreases as a power-law $\sim (s - s^*)^{-1/2}$ for $s \approx s^*$ (see inset).

$s \gg s^*$. Using a numerical integration of (23), for different choices of the parameters, we find that, for $s > s^*$, the transition time t_m (minima of the strain rate) is always equal to $t_c/2$, as for the 2 previous models. This result recovers the proportionality of t_m and t_c found experimentally, but predicts a shorter duration for the primary creep ($t_c/2$) than the observations ($t_m \approx 2t_c/3$, see Figure 14).

This model explains qualitatively the existence of both the power-law decrease of the strain rate during the primary creep regime and the power-law singularity before failure. It also explains the p-value of the primary creep, which ranges in the model between 0 and 1 as a function of the applied stress. The larger the stress, the smaller the apparent p-value, and the smaller the failure time and the duration of the primary creep. If the stress is too large, we do not observe the first primary creep regime and the strain rate continuously accelerates before failure. The model thus explains the correlation observed between the p-value and the failure time shown in Figure 15e.

We have also studied a more complex model with RE elements that obeys Burger's topology, in an effort to explain the value $p' < 1$ found experimentally. Each RE element is composed of a Kelvin element (spring and dashpot in parallel) associated in series with a Maxwell element (spring and dashpot in series). The strain rate in now the sum of the two contributions of the Maxwell and Kelvin element. We found that adding the Maxwell element in parallel does not change qualitatively the behavior of the model. If the strain rate of Maxwell's element is similar to the strain rate of the Kelvin element, we observe close to failure an apparent power-law with an exponent $p' < 1$, but for a limited time-range (no more than one order of magnitude in time), which evolves toward a pure power-law with $p' = 1$ close to failure.

5 Conclusion

We have performed creep experiments on fiber composites. We have established experimentally the existence of power-law relaxations both for the strain (Andrade's law) and for the acoustic emissions (analog of Omori's law for earthquakes) in the primary creep regime. We also observed a power-law singularity both for the strain rate and for the rate of AE in the tertiary regime culminating in global

failure. Our experiments confirm over large time scales covering up to 4 orders of magnitude in time previous announcement of power laws in the tertiary creep regime, which were established over more limited time scales (Guarino et al., 2002).

We have shown the correlations between the p-exponent of the primary creep regime and the rupture time t_c. We have also shown a strong correlation of t_c with the time t_m of the minimum strain rate in the secondary creep regime. These results suggest interesting possibilities for the prediction of the rupture time t_c. We have developed a simple model of representative elements, made of a spring in parallel with a linear or nonlinear dashpot, interacting via democratic load sharing. Our model recovers all the observations apart from the exact value of p', which is found experimentally to be ≈ 0.8, smaller than the value $p' \approx 1$ found in the model. An essential ingredient for the observation of the power-law singularity of the strain rate before failure is a large heterogeneity of the rupture thresholds of the representative elements. We stress that the interactions between the RE elements together with a large heterogeneity and a simple rheology is sufficient and replaces the need for complex memory effects. In particular we do not need to invoke the integro-differential Schapery long-memory formalism (Cardon et al., 2000; Ségard et al., 2002).

A natural improvement of the model would be to relax the democratic load sharing rule a la DFBM, along the work of Kun et al. (2003). These authors show interesting new effects in the creep dynamics of Model 1 when introducing realistic elastic interaction with an elastic Green function decaying as a power law of the distance between elements. We expect that this improvement will provide a more realistic value of p' of the strain in the tertiary creep regimes.

We end by on a conceptual note. The model presented here is a macroscopic deterministic effective description of the experiments. In contrast, the modeling strategy of Ciliberto et al. (2001), Politi et al. (2002) and Saichev and Sornette (2003) emphasizes the interplay between microscopic thermal fluctuations and frozen heterogeneity. Qualitatively, our models are similar to a deterministic macroscopic Fokker-Planck description while the thermal models of Ciliberto et al. (2001), Politi et al. (2002) and Saichev and Sornette (2003) are reminiscent of stochastic Langevin models. It is well-known in statistical physics that Fokker-Planck equations and Langevin equations are exactly equivalent for systems at equilibrium and just constitute two different descriptions of the same processes, and their correspondence is associated with the general fluctuation-dissipation theorem. Similarly, the encompassing of both the Andrade relaxation law in the primary creep regime and of the time-to-failure power law singularity in the tertiary regime by our model 3 and by the thermal model as shown by Saichev and Sornette (2003) suggests a deep connection between these two levels of description for creep and damage processes.

References

[1] Agbossou, A., Cohen I., Muller, A., 1995. Effects of interphase and impact strain rates on tensile off-axis behaviour of unidirectional glass fibre composite: experimental results, Engineering Fracture Mechanics 52 (5), 923-935.

[2] Andersen, J.V., Sornette D., Leung, K.-T., 1997. Tri-critical behavior in rupture induced by disorder, Phys. Rev. Lett. 78, 2140-2143.

[3] Andrade, E. N. da C., 1910. The Viscous Flow in Metals, and Allied Phenomena, Proc. R. Soc. A 84, 1-12.

[4] Anifrani, J.-C., Le Floc'h, C., Sornette, D., Souillard, B., 1995. Universal Log-periodic correction to renormalization group scaling for rupture stress prediction from acoustic emissions, J. Phys. I France 5 (6), 631-638.

[5] Astarita, G., Marrucci, G., 1974. Principles of Non-Newtonian Fluid Mechanics, McGraw-Hill, London.

[6] Awerbuch, J., Ghaffari, S., 1988. Monitoring progression of matrix splitting during fatigue loading through acoustic emission in notched unidirectional graphite/epoxy composite, Journal of Reinforced Plastics and Composites 7 (3), 245-264.

[7] Bakuckas, J.G., Jr., Prosser, W.H., Johnson, W.S., 1994. Monitoring damage growth in titanium matrix composites using acoustic emission, Journal of Composite Materials 28 (4), 305-328.

[8] Batdorf, S.B., Ghaffarian, R., 1982. Tensile strength of unidirectionally reinforced composites, Journal of Reinforced Plastics and Composites 1, 153-176.

[9] Beattie, A.G., 1983. Acoustic Emission, principles and instrumentation. J. of Acoustic Emission, 2(2/1), 95-128.

[10] Cardon, A.H., Qin, Y., Van Vossole C., Bouquet, P., 2000. Prediction of the Residual Structural Integrity of a Polymer Matrix Composite Construction Element, Mechanics of Time-Dependent Materials 4, 155-167.

[11] Chang, C., Sun, C.T., 1988. Acoustic emissions and transient elastic waves in an orthotropic laminate plate, Composite Science and Technology 33 (3), 213-236

[12] Ciliberto, S., Guarino A., Scorretti, R., 2001. The effect of disorder on the fracture nucleation process, Physica D 158 (1-4), 83-104.

[13] Czochralski, J., 1916. Die Metallographie des Zins und die Theorie des Formanderung beldsamer Metalle, Metal und Erz, XIII (N.F.IV) (18), 381-393.

[14] Daniels, H. A., 1945. The statistical theory of the strength of bundles of thread, Proc. Soc. London, Ser. A 183, 405-435.

[15] Dzenis, Y., Qian, J., 1998. Extraction of histories of damage micromechanics in unidirectional composites by acoustic emission technique, International Conference on Advanced Composites ICAC'98, Eds. Gowayed, Y. and Abd El Hady, F.

[16] Dzenis Y., Qian, J., 2001. Analysis of microdamage evolution histories in composites. Int. J. of Solids and Struct. 38 (10-13), 1831-1854.

[17] El Guerjouma, R., Baboux, J.C., Ducret D., Godin N., Guy P., Huguet S., Jayet Y., Monnier T., 2001. Non-destructive evaluation of damage and failure of fiber reinforced polymer composites using ultrasonic waves and acoustic emission' Advanced Engineering Materials, 3(8), 601-608.

[18] Ely, T.M., Hill, E.K., 1995. Longitudinal splitting and fibre breakage characterisation in graphite epoxy using acoustic emission data, Material Evaluation, 53(2), 288-294.

[19] Förster, F., Scheil, E., 1934. Akustische untersuchung der bildung von martensitnadeln, Zeitschrift für Metallkunde, 28 (9), 245-247.

[20] Garcimartin, A., Guarino, A., Bellon, L., Ciliberto, S., 1997. Statistical properties of fracture precursors, Phys. Rev. Lett. 79 (17), 3202-3205.

[21] Goretta, K. C., Cruse, T. A., Koritala, R. E., Routbort, J. L., Mélendez-Martínez, J. J., de Arellano-López, A. R., 2001. Compressive creep of polycrystalline ZrSiO4, Journal of the European Ceramic Society, 21 (8), 1055-1060.

[22] de Groot, P.J., Wijnen, P.A.M., Janssen, R.B.F., 1995. Real-time frequency determination of acoustic emission for different fracture mechanisms in carbon/epoxy composites, Composite Science and Technology 55 (4), 405-412.

[23] Guarino, A., Ciliberto, S., Garcimartin, A. Zei, M., Scorretti, R., 2002. Failure time and critical behaviour of fracture precursors in heterogeneous materials, Eur. Phys. J. B. 26 (2), 141-151.

[24] Helmstetter A., Sornette S., Grasso J.-R., 2003. Mainshocks are aftershocks of conditional foreshocks: How do foreshock statistical properties emerge from aftershock laws, J. Geophys. Res., 108, 2046, doi:10.1029/2002JB001991.

[25] Hidalgo, R.C., Kun, F., Herrmann, H.J., 2002. Creep rupture of viscoelastic fiber bundles, Phys. Rev. E. 65 (3), 032502/1-4.

[26] Hoffmann, M. J., Hammer, M., Endriss, A., Lupascu, D. C., Correlation between microstructure, strain behavior, and acoustic emission of soft PZT ceramics, Acta Materialia, 49(7), 1301-1310.

[27] Huguet, S., Godin, N., Gaertner, R., Salmon, L., Villard, D., 2002. Use of acoustic emission to identify damage modes in glass fibre reinforced polyester using SOFM signal classification, Composites Science and Technology, 62, (10-11), 1433-1444.

[28] Ishikawa, K., Maehara, M., Kobayashi. Y., 2002. Mechanical modeling and microstructural observation of pure aluminum crept under constant stress, Materials Science and Engineering A322 (1-2), 153-158.

[29] Jaumé S. C. Sykes, L.R., 1999. Evolving towards a critical point: A review of accelerating seismic moment/energy release prior to large and great earthquakes, Pure Appl. Geophys. 155, 279-306.

[30] Johansen, A., Sornette, D., 2000. Critical ruptures, Eur. Phys. J. B 18 (1), 163-81

[31] Kagan Y. Y., 1999. Universality of Seismic Moment-frequency Relation, Pure Appl. Geophys. 155, 537-573.

[32] Kaiser, J., 1950. Untersuchungen uberdas Auftreten Gerauschen beim Zugversuch, Dr. Ing. Dissertation, Techniche Hochshule München.

[33] Kloua, H., Maslouhi, A., Roy, C., 1995. Monitoring of free edge delamination in graphite epoxy laminates under fatigue loading, Canadian Aeronautics and Space Journal 41, 21.

[34] Kuhn, M.R., Mitchell, J.K., 1993. New perspective on soil creep, J. Geotechnical Engineering, 119 (3), 507-524.

[35] Kun, F., Moreno, Y., Hidalgo, R.C., Herrmann, H.J., 2003. Creep rupture has two universality classes, Europhysics Letters 63 (3), 347-353.

[36] Liu, J.Y., Ross, R.J., 1996. Energy criterion for fatigue strength of wood structural members, Journal of Engineering Materials and Technology 118 (3), 375-378.

[37] Lockner, D. A., 1998. A generalized law for brittle deformation of Westerly granite, J. Geophys. Res. 103 (B3), 5107-5123.

[38] Luo, J.-J., Wooh, S.-C., Daniel, I.M., 1995. Acoustic emission study of failure mechanisms in ceramic matrix composite under longitudinal tensile loading, Journal of Composite Materials 29 (15), 1946-1961.

[39] Ma, X. Q., Takemoto, M., 2001. Quantitative acoustic emission analysis of plasma sprayed thermal barrier coatings subjected to thermal shock tests, Materials Science and Engineering A, 308(1-2), 101-110.

[40] Main, I. G., 2000. A damage mechanics model for power-law creep and earthquake aftershock and foreshock sequences, Geophys. J. Int. 142(1), 151-161.

[41] Miguel, M.C., Vespignani, A. Zaiser, M. Zapperi, S., 2002. Dislocation jamming and Andrade creep, Phys. Rev. Lett. 89 (16), 165501.

[42] Morita K., Hiraga, K., 2002. Critical assessment of high-temperature deformation and deformed microstructure in high-purity tetragonal zirconia containing 3 mol.% yttria, Acta Materialia, 50 (5), 1075-1085.

[43] Moura, A., Yukalov, V. I., 2002. Self-similar extrapolation for the law of acoustic emission before failure of heterogeneous materials, Int. J. Fract. 118 (3), 63-68.

[44] Mukhopadhyay, C. K,. Ray, K. K., Jayakumar, T., Raj, B., 1989. Acoustic emission from tensile deformation of unnotched and notched specimens of AISI type 304 stainless steels, Materials Science and Engineering A, 255(1-2), 98-106.

[45] Nielsen, A., 1989. Acoustic emission from steel structures, Journal of Acoustic Emission 8 (1-2), 557-561.

[46] Omori, F., 1894. On the aftershocks of earthquakes, J. Coll. Sci. Imp. Univ. Tokyo, 7, 111-120.

[47] Ono, K., Huang, Q., 1996. Personal communication.

[48] Pisarenko, V.F. Sornette, D., 2003. Characterization of the frequency of extreme earthquake events by the generalized Pareto distribution, Pure Appl. Geophys. 60, 2343-2364.

[49] Politi, A., Ciliberto, S., Scorretti, R., 2002. Failure time in the fiber-bundle model with thermal noise and disorder, Phys. Rev. E 66 (2), 026107/1-6.

[50] Portevin, A., Le Chatelier, F., 1923. Tensile tests of alloys undergoing transformation, Comptes-rendus Acad. Des Sciences, 176, 507-510.

[51] Pradhan, S., Chakrabarti, B.K., 2004. Failure properties of fiber bundle models, (http://arxiv.org/abs/cond-mat/0307734)

[52] Prosser, W.H., Jackson K.E., Kellas S., Smith B.T., MacKeon J., Friedman A., 1995. Advanced waveform-based acoustic emission detection of matrix cracking in composites, Material Evaluation, 53 (9) 1052-1058.

[53] Reifsnider, K.L., Lesco, J., Case, S., 1995. Kinetic methods for predictions of damage tolerance of high temperature polymer composites, in COMPOSITES95: Recent Advances in Japan and the United States, I. Kimpara, H. Miyairi, N. Takeda, Eds., Proceedings Japan U.S. CCM VII, Kyoto, 49-55.

[54] Reurings, F., Alava, M.J., 2004. Damage growth in random fuse networks, preprint at http://arXiv.org/abs/cond-mat/0401592.

[55] Roberts, T.M., Talebzadeh, M. (2003) Fatigue life prediction based on crack propagation and acoustic emission count rates, Journal of Constructional Steel Research, 59 (6), 679-694.

[56] Roux, S., Hild, F., 2002. On the relevance to meanfield in continuous damage mechanics, Int. J. Fract. 116 (3), 219-229

[57] Saichev, A., Sornette, D., 2003. Andrade, Omori and time-to-failure laws from thermal noise in material rupture, preprint http://arXiv.org/abs/cond-mat/0311493.

[58] Sammis S.G., Sornette D., 2002. Positive Feedback, Memory and the Predictability of Earthquakes, Proceedings of the National Academy of Sciences USA 99, SUPP1, 2501-2508.

[59] Ségard, E., Benmedakhene, S., Laksimi A., Laï, D., 2002. Influence of the fibre-matrix interface on the behaviour of polypropylene reinforced by short glass fibres above glass transition temperature, Composites Science and Technology 62 (15), 2029-2036.

[60] Shcherbakov, R., Turcotte, D.L., 2003. Damage and self-similarity in fracture, Theoretical and Applied Fracture Mechanics 39 (3), 245-258.

[61] Shiwa, M., Carpenter, S., Kishi, T., 1996. Analysis of acoustic emission signals generated during the fatigue testing of GFRP, Journal of Composite Materials 30(18), 2019-2041.

[62] Singh, S.K., Srinivasan K., Chakraborty D., 2003. Acoustic emission studies on metallic specimen under tensile loading, Materials and Design, 24(6), 471-481.

[63] Sornette, D., Vanneste, C., 1992. Dynamics and memory effects in rupture of thermal fuse networks, Phys. Rev. Lett. 68 (5), 612-615.

[64] Sornette, D. and Vanneste C., 1994. Dendrites and fronts in a model of dynamical rupture with damage. Phys. Rev. E, 50, 4327-4345.

[65] Turcotte, D.L., Newman W.I., Shcherbakov, R., 2003. Micro and macroscopic models of rock fracture, Geophys. J. Int. 152 (3), 718-728.

[66] Vanneste, C., Sornette, D., 1992. Dynamics of rupture in thermal fuse models, J. Phys. I France 2, 1621-1644.

[67] Vujosevic, M., Krajcinovic, D., 1997. Creep rupture of polymers – A statistical model, Int. J Solid Structures 34 (9), 1105-1122.

[68] Watanabe, M., Okabe, T., Enoki, M., Kishi, T., 2003. Evaluation of in situ fracture toughness of ceramic coatings at elevated temperature by AE inverse analysis, Science and Technology of Advanced Materials, 4(2), 205-212.

[69] Williams, R.S., Reifsnider, K.L., 1974. Investigation of acoustic emission during fatigue loading of composite specimens, Journal of Composite Materials 8, 340-355.

[70] Yamaguchi, K., Oyaizu, H., Johkaji, J., Kobayashi, Y., 1991. In Acoustic Emission: Current Practice and Future Directions, Sachse, W., Roget, J., Yamaguchi, K. (Eds.), ASTM STP 1077 American Society for Testing and Materials, Philadelphia, p. 123.

[71] Yukalov, V.I., Moura A., Nechad, H., 2004. Self-similar law of energy release before materials fracture, J. Mech. Phys. Solids 52, 453-465.